Asian Journal of Nanoscience and Materials, 2019, 2(2), 159-185.

Full article

TD-DFT Calculations, Electronic Structure, NBO, NLO Analysis, Biological Activity, and Electronic Absorption Spectra of Some Novel Schiff base Derivatives

Shimaa Abdel Halim[a,*], Esam A. Gomaa[b], Shymaa E. Rashed[b]

[a]*Department of Chemistry, Faculty of Education, Ain Shams University, Roxy 11711, Cairo, Egypt.*

[b]*Department of Chemistry, Faculty of Science, Mansoura University, Mansoura. Egypt.*

Received: 12 October 2018, Revised: 12 November 2018 and Accepted: 16 November 2018.

ABSTRACT: The electronic structure and spectra of the schiff base derivatives compounds were investigated using TD-DFT/B3LYB/6-311G (d, p) level of theory. The results showed that all the studied compounds 1–4 were non-planar, as indicated from the dihedral angles. The electronic absorption spectra of the studied compounds were recorded in the UV-VIS region, in both ethanol (as polar solvent) and dioxane (as non-polar solvent). Solvent dependence of the band maxima (λmax) and intensities of the observed spectra are explained in terms of blue and red shifts. Electronic configurations contributing to each excited state are identified and the relevant MOs are characterized. The theoretical spectra computed at CAM-B3LYP/6-311G (d, p) in gas phase, ethanol and dioxane nicely reproduce the observed spectra. The natural bond orbital (NBO) analysis were discussed in terms of the extent of delocalization, intermolecular charge transfer, and second order perturbation interactions between the donor and acceptor MOs. The calculated EHOMO and ELUMO energies of the studied compounds can be used to explain the extent of charge transfer in the molecule and to calculate the global properties; the chemical hardness (η), global softness (S), electrophilicity (ω), and electronegativity (χ). The calculated nonlinear optical parameters (NLO); polarizibilty (α), anisotropy of the polarizibility (Δα) and first order hyperpolarizibility (β) of the studied compounds have been calculated at the same level of theory and compared with the proto type Para-Nitro-Aniline (PNA), show promising optical properties. 3D-plots of the molecular electrostatic potential (MEP) for some of the studied compounds are investigated and analyzed showing the distribution of electronic density of orbital's describing the electrophilic and nucleophilic sites of the selected molecules. The biological activity of the studied compounds was tested against gram positive, gram negative and Fungi. A correlation between energetic, global properties and biological activity were investigated and discussed..

KEYWORDS: UV spectra; TD-DFT; NBO and NLO analysis; Biological activity; Schiff base derivatives.

***Corresponding author: Mohammad Rabiee, Email: mrabiee@aut.ac.ir , Tel.: +98(21)64542381

Asian Journal of Nanoscience and Materials

1. Introduction

Schiff bases are condensation products of primary amines with carbonyl compounds and they were first reported by Schiff [1] in 1864. Several studies [2-8] showed that the presence of a lone pair of electrons in a sp^2 hybridized orbital of nitrogen atom of the azomethine group is of considerable chemical and biological importance. Schiff bases also show some analytical applications [9]. Schiff bases are characterized by the -N=CH- (imine) group which imports in elucidating the mechanism of transamination and rasemination reaction in biological system [10, 11]. Schiff bases have been studied for their important properties in catalysis [12]. They showed catalytic activity in hydrogenation of olefins [13]. Schiff bases have been reported in their biological properties, such as, antibacterial, antifungal activities [14-17]. Their metal complexes have been widely studied because they have anticancer and herbicidal applications [18, 19]. I satin Schiff bases were reported to possess antiviral, anti-HIV, antiprotozoal and anthelmintic activities [20]. They also exhibit significant anticonvulsant activity, apart from other pharmacological properties [21].

The electronic absorption and emission spectra manifests the electronic structure and spectra of molecules. Theses according to understanding of the forces that govern the electronic structure of the proposed molecules. Now there is no systematic study of substituent and solvent effects on the observed spectra of compounds 1-4. Such a study is very important in understanding their electronic structure which may correlate with their biological activity.

The newly synthesized compounds 1-4 are expected to have biological potential which needs to be explored by investigating their electronic structure and spectra experimentally and theoretically. The UV spectra, NLO and NBO analysis have been used to explain charge transfer within these molecules. The solvatochromism PCM is dependence of the electronic transitions of these molecules on the polarity of the solvent can be inferred from solvent-induced changes of such transitions.

In the literature, no systematic study conducted on the electronic structure, substituent effect and bonding characteristics of the studied compounds.

Asian Journal of Nanoscience and Materials

Therefore, our study is to shed more light on the geometrical parameters (bond lengths, bond angles and dihedral angles), ground state properties of the compounds **1-4**, energy gaps (highest occupied molecular orbital [HOMO]–lowest unoccupied molecular orbital [LUMO]), natural charges, and electrostatic potential. In addition, these are calculated using B3LYP/6-311G (d, p). The electronic dipole moment (μ), and first order hyperpolarizibility (β) values of the studied compounds have been computed to study the NLO properties to identify and characterize the forces that govern the structure-activity and the optical properties of the studied compounds. Finally, global reactivity descriptors including electronegativity (X), hardness (η), softness (S), and electrophilicity ***(ω)*** of the studied compounds were calculated and analyzed, while molecular electrostatic potential (MEP) of molecules were explored as well and The experimental (UV) using TD-DFT and theoretical electronic structure of compounds **1-4** using CAM- B3LYP/6-311G (d, p). Also; studied the structure activity relationship (SAR) by using the antimicrobial activity application for the compounds **1-4**. The contributing configurations and MOs are characterized using the origin of each absorption band. The charge transfer of the electron density in the studied molecular systems are characterized by natural bond orbital analysis (NBO) and identify the extent of delocalization of conjugative interaction between different subsystems of the studied compounds. The effect of the solvent polarity on the observed spectra and hence, predicting the relative stabilities, extent of charge transfers character and assignment of the observed electronic transitions are analyzed.

2. Experimental

2.1. Compounds

The structure of the four proposed molecules **1–4**, is shown in Figure …, where compound **1** is 4-(2-(4-nitrophenyl)ethylidene) aminohippurate, compound **2** is 4-(2-(N,N-dimethylephenyl)ethylidene)aminohippurate, compound **3** is 4-(2-(4-chlorophenyl)ethylidene)aminohippurate, compound **4** is 4-(2-(3-hydroxy-4-methoxyphenyl) ethylidene) aminohippurate.

Asian Journal of Nanoscience and Materials

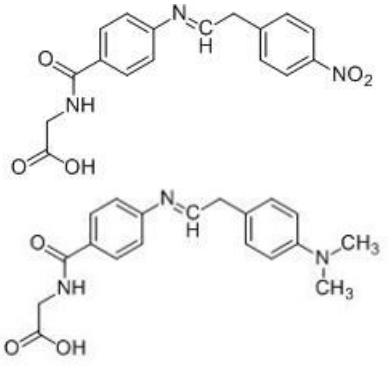

(1)

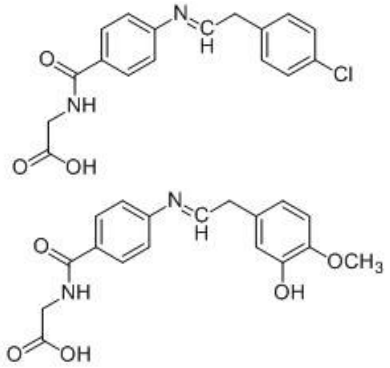

(2)

(3)

(4)

2.2. Solvents

Polar (ethanol) and non-polar (dioxane) solvents were obtained from Merck, AR- grade, and used without further purification.

2.3. Apparatus

A Perkin Elmer lambda 4B spectrophotometer using 1.0 cm fused quartz cells were used to measured the electronic absorption spectra over the range 200-900 nm.

2.4. Antimicrobial Study

Biological activities of synthesized compounds **1-4** were studied for antibacterial and antifungal properties against different types of bacteria; Gram positive S. aureus, and B.subtillis and Gram-negative E. coli (Escherichia coli) and Pseudomonas aeuroginosa, and C. albicans and A. flavus for fungus.

2.5. Computational Details

All computations were carried out using Khon-Sham's DFT method subjected to the gradient-corrected hybrid density functional B3LYP method [22]. This function is a combination of the Becke's three parameters non-local exchange potential with the non-local correlation functional of Lee et al [23]. For each structure, a full geometry optimization was performed using this function [23] and the 6-311G (d, p) bases set [24] as implemented by Gaussian 09 package [25]. All geometries were visualized either using GaussView 5.0.9 [26] or chemcraft 1.6 [27] software packages. No symmetry constrains were applied during the geometry optimization. Also, the total static dipole moment (μ), $\langle\Delta\alpha\rangle$, and $\langle\beta\rangle$, values were calculated by using the following equations [28-30]:

Asian Journal of Nanoscience and Materials

$$\mu = (\mu^2_x + \mu^2_y + \mu^2_z)^{1/2},$$

$$\langle\alpha\rangle = 1/3\,(\alpha_{xx} + \alpha_{yy} + \alpha_{zz}),$$

$$\Delta\alpha = \left((\alpha_{xx} - \alpha_{yy})^2 + (\alpha_{yy} - \alpha_{zz})^2 + (\alpha_{zz} - \alpha_{xx})^2/2\right)^{1/2},$$

$$\langle\beta\rangle = (\beta^2_x + \beta^2_y + \beta^2_z)^{1/2},$$

(1)

Where

$$\beta_x = \beta_{xxx} + \beta_{xyy} + \beta_{xzz},$$

$$\beta_y = \beta_{yyy} + \beta_{xxy} + \beta_{yzz},$$

$$\beta_z = \beta_{zzz} + \beta_{xxz} + \beta_{yyz}.$$

(2)

HOMO and LUMO energy values, electronegativity, and chemical hardness can be calculated as follows: $\chi = (I + A)/2$ (electronegativity), $\eta = (I - A)/2$ (chemical hardness), $S = 1/2\eta$ (global softness), $\omega = \mu^2/2\eta$ (electrophilicity) where I and A are ionization potential and electron affinity, and $I = -E_{HOMO}$ and $A = -E_{LUMO}$, respectively [31, 32]. The electronic transition properties which include the maximum excitation wavelength (λ_{max}) and relative intensities (oscillator strengths, f), were obtained by the time dependant density functional theory (TD-DFT), [33] using "A new hybrid exchange-correlation functional using the Coulomb-attenuating method (CAM-B3LYP)," at the 6-311G (d, p) bases set [34]. The population analysis has also been performed by the natural bond orbital method [35] at B3LYP/6-311G (d, p) level of theory using natural bond orbital (NBO) under Gaussian 09 program package. The second-order Fock matrix was used to evaluate the donor-acceptor interactions in the NBO basis [36]. For each donor (i) and acceptor (j), the stabilization energy $E^{(2)}$ associated with the delocalization $i \rightarrow j$ is estimated as

$$E^{(2)} = \Delta E_{ij} = q_i\,(F(ij)^2/\varepsilon_j - \varepsilon_i),$$

(3)

where q_i is the donor orbital occupancy, ε_i and ε_j are diagonal elements and $F(ij)$ is the off-diagonal NBO Fock matrix element. For the conversion factors of α, β, and HOMO and LUMO energies in atomic and cgs units: 1 atomic unit (a.u.) = 0.1482×10^{-24} electrostatic unit (esu) for polarizability $\langle\alpha\rangle$; 1 a.u. = 8.6393×10^{-33} esu for first hyperpolarizability $\langle\beta\rangle$; 1 a.u. = 27.2116 eV for HOMO and LUMO energies.

3. Result and Discussion:

3. 1. Electronic Structure

3.1.1. Geometry Structure

Figure 1 presents the optimized structures and the vector of the dipole moment of the studied compounds 1-4 using the B3LYB/6-311G (d, p). The energies of HOMO, LUMO, energy gap, and dipole moment of all compounds are shown in Figure 2 and Table 3. The optimized geometrical parameters (bond lengths, bond angles and dihedral angles) of the studied compounds 1-4 is listed in Table 1 and 2. . The most stable geometry of the studied compounds, 1-4, is the non-planar structures as indicated from the dihedral angles (Table 2). The optimized bond length of carbon-carbon in the benzo rings fall in the range from 1.3798 to 1.5506 Å in the studied compounds 1-4 (Table 1). The compound shows no extended conjugation involving the carbon-carbon bonds, since the C-C and C=C bond lengths are significantly larger and shorter, respectively, than the C-C bond lengths in a typical aromatic six-member ring (Ca. 1.39 Å). Indeed, the C-C bond lengths in the studied compounds 1-4 (1.403-1.482 Å) were found to be similar to the central bond in butadiene (1.463 Å) [37], while the C=C bond lengths (1.389-1.398 Å) do not differ very much from the C=C bond length in ethylene [38]. These conclusions are suggested by the considerably large O-C bond lengths and shorten C=O bond length (Table 1). The computed bond angles are largely affected by the presence of C=O group in C-4, especially <O1C2C4, <H25O3C2, <C3C4N5, and <C16C17H34, angles (Table 1). The optimized of the dihedral angles of the studied compounds 1-4 not near 0.0 and 180° indicating that, these compounds 1-4 are planar structure (Table 2).

3.1.2. Ground State Properties

The ionization energy, I.E, of compounds **1-4** which measures the donating property (oxidation power) (c.f. Table 3) follows the order: **1 > 3 > 4 > 2** as shown in Table 3 and Figure 2. However the electron affinity, E.A. reveals the accepting property (reducing power). The order of accepting properties of compounds **1-4** follows **1 < 3 < 4 < 2** as shown in Table 3 and Figure 2. The band gap, E_{gap}, is the energy gap between E_{HOMO} and E_{LUMO}, it signifies the facile electron transition from E_{HOMO} to E_{LUMO},

Asian Journal of Nanoscience and Materials

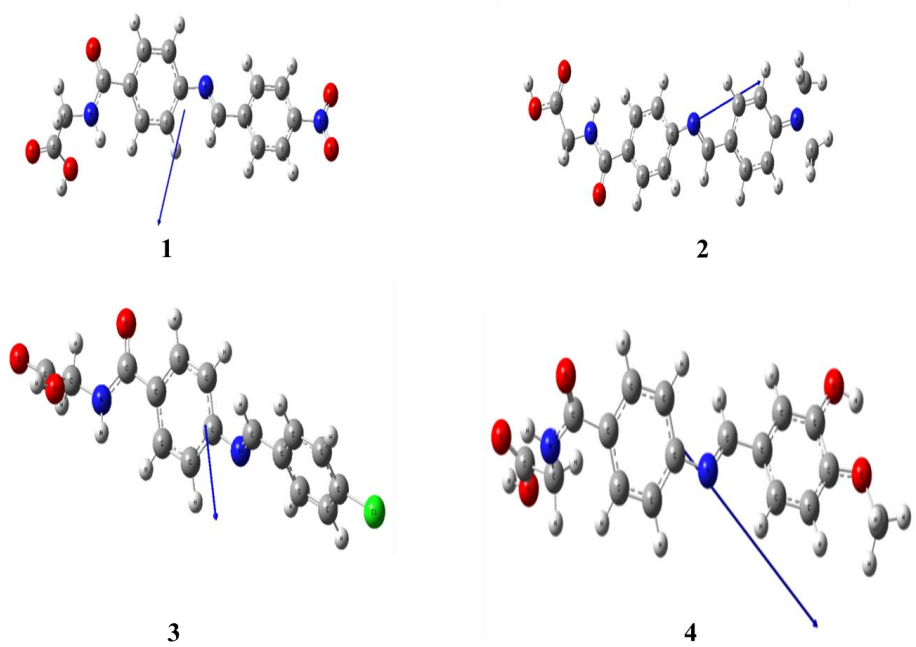

Fig. 1. The optimized structure, perspective view of dipole moment of the studied compounds **1-4** at B3LYP/6-311G (d, p).

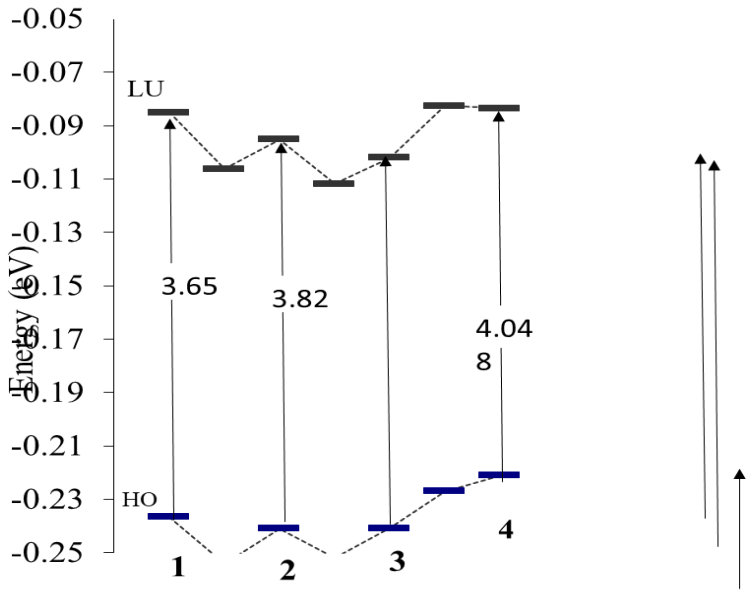

Fig. 2. Energy of HOMO, LUMO and energy gap of the studied compounds **1-4** at B3LYP/6-311G (d, p) level of theory.

Asian Journal of Nanoscience and Materials

1	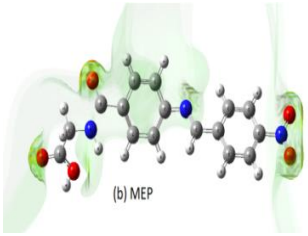	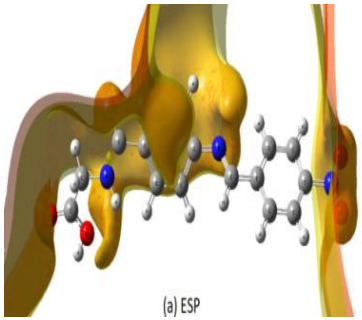	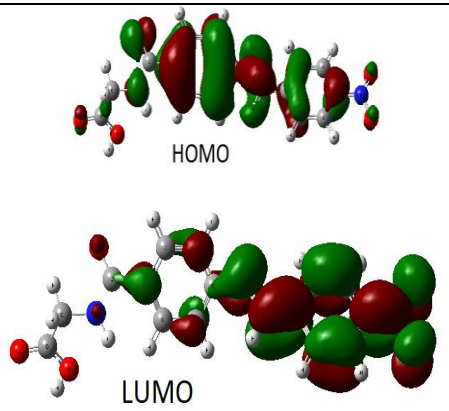
	MEP	ESP	HOMO LUMO
2	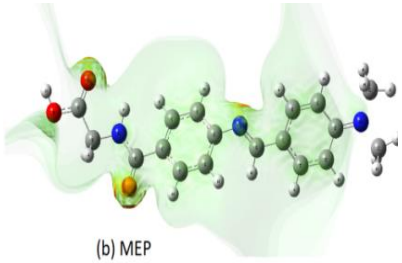	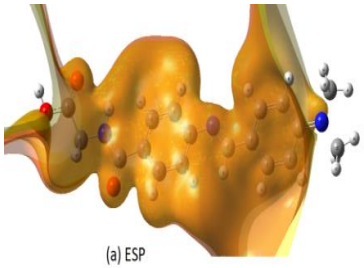	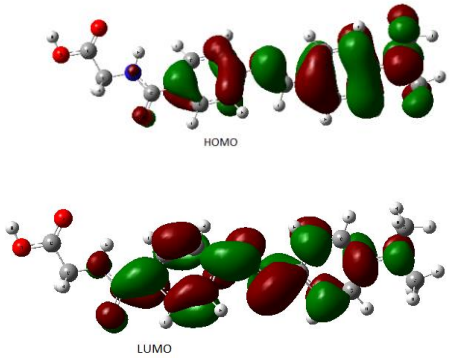
	MEP	ESP	HOMO LUMO

Asian Journal of Nanoscience and Materials

3	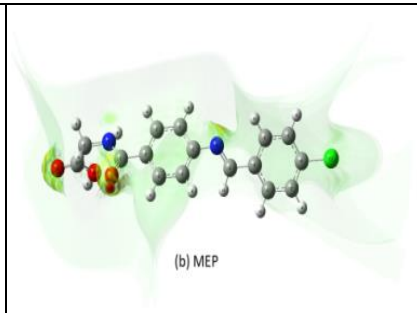	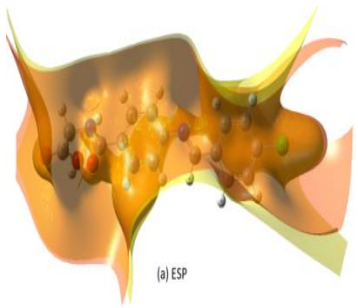	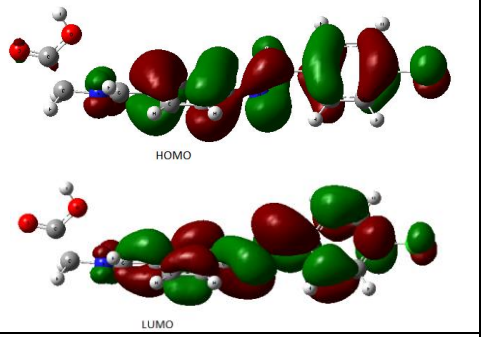
	MEP	ESP	HOMO LUMO
4	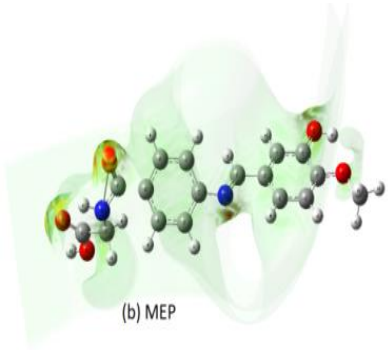	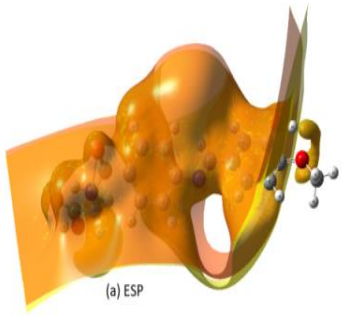	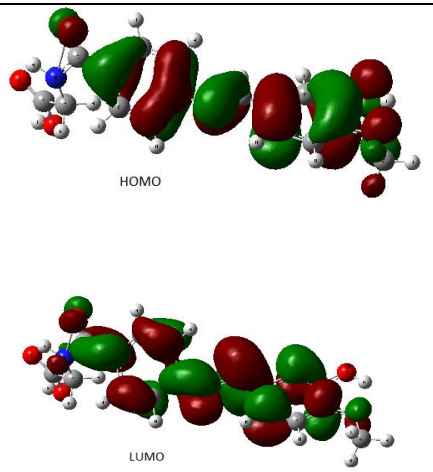
	MEP	ESP	HOMO LUMO

Fig.3. Molecular surfaces of studied compounds **1-4** at B3LYP/6-311G (d, p).

Asian Journal of Nanoscience and Materials

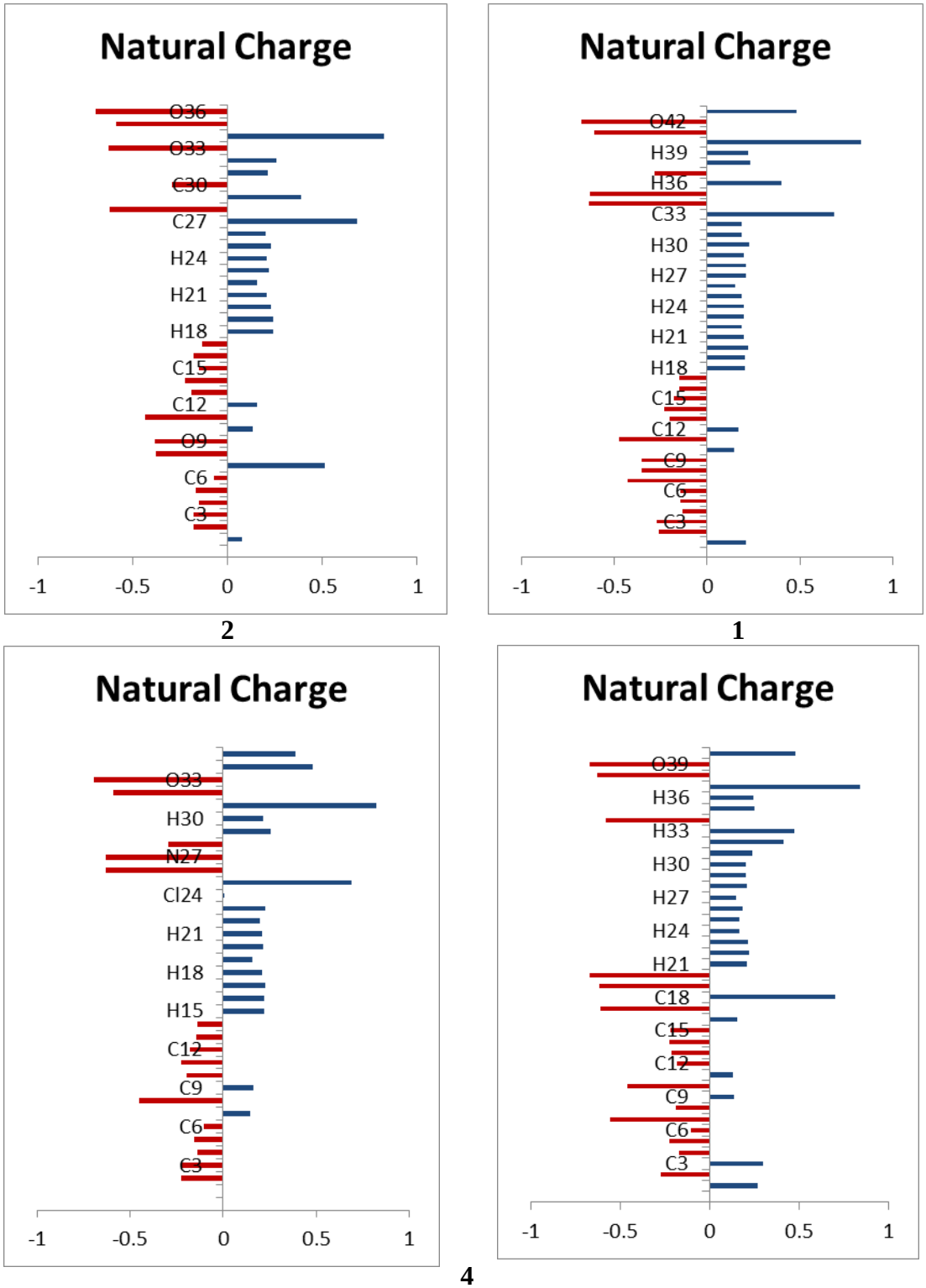

Atomic charge distribution

Fig.4. Atomic charge distribution (au) for studied compounds **1-4** at B3LYP/6-311G(d,p) basis set.

Asian Journal of Nanoscience and Materials

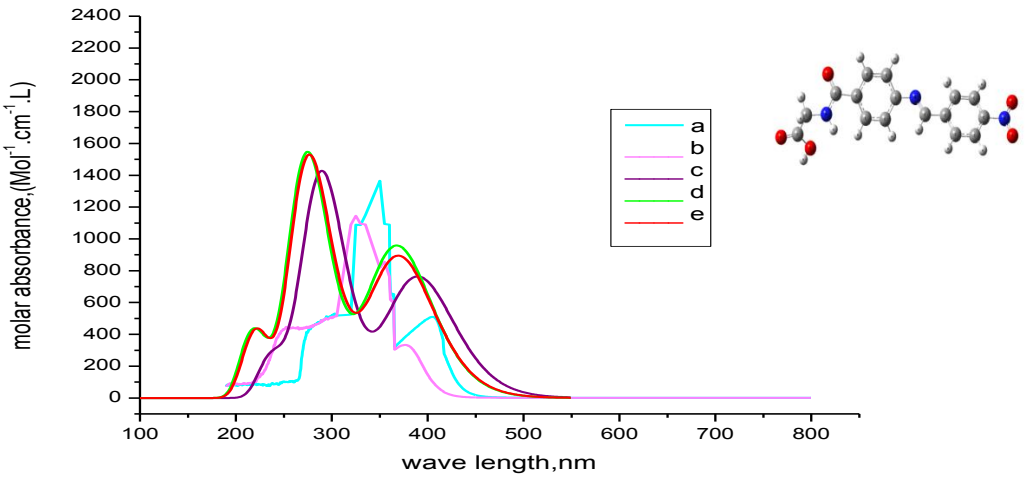

Fig. 5. Electronic absorption spectra of **1**,(a) experimental in benzene, (b) experimental in ethanol, (c) theoretical in gas phase, (d) theoretical in benzene, (e) theoretical in ethanol.

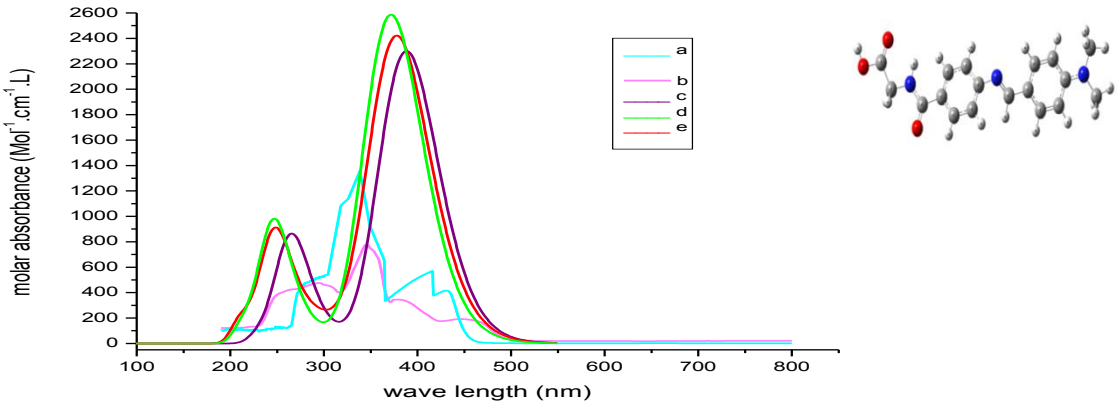

Fig. 6. Electronic absorption spectra of **2**,(a) experimental in benzene, (b) experimental in ethanol, (c) theoretical in gas phase, (d) theoretical in benzene, (e) theoretical in ethanol.

Asian Journal of Nanoscience and Materials

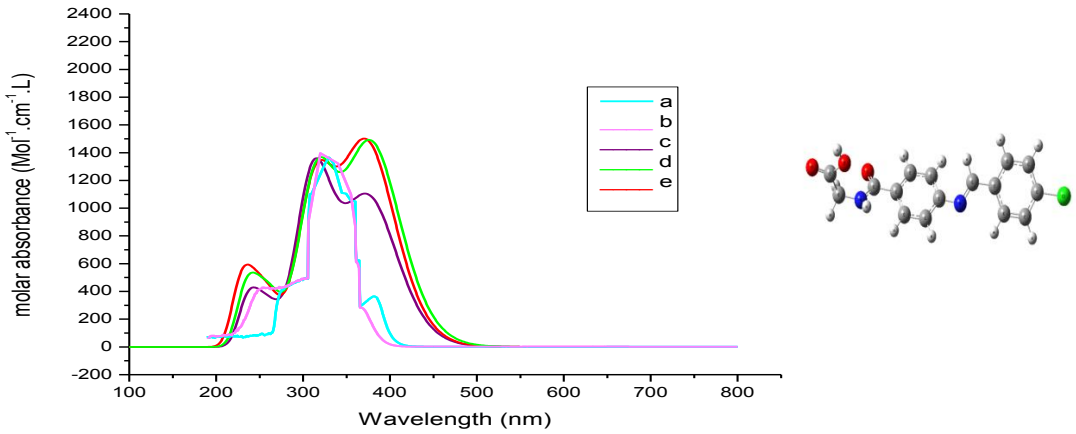

Fig. 7. Electronic absorption spectra of **3**,(a) experimental in benzene, (b) experimental in ethanol, (c) theoretical in gas phase, (d) theoretical in benzene, (e) theoretical in ethanol.

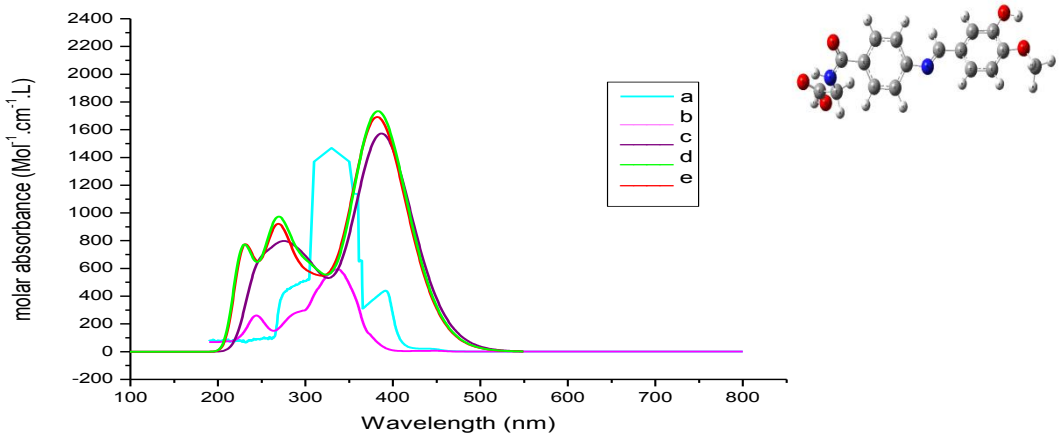

Fig. 8. Electronic absorption spectra of **4**,(a) experimental in benzene, (b) experimental in ethanol, (c) theoretical in gas phase, (d) theoretical in benzene, (e) theoretical in ethanol.

Asian Journal of Nanoscience and Materials

i.e. the reactivity of molecules in the studied compounds **1-4** are governed by their chemical structures. The results in Table 3 and Figure 2 shows that the computed reactivity in the gas phase of the studied compounds increases in the order: **1 > 2 > 4 > 3**. This indicates that the smaller the E_{gap}, the higher the reactivity of these compounds. Finally, the theoretically computed dipole moment, μ measures the charge separation over the molecule. The general trend of the dipole moment changes for the studied compounds **1-4** follow the order **4 > 2 > 1 > 3** (c.f. Table 3) and the vector of the dipole moment is presented in Figure 1.

3.1.3. Global Reactivity Descriptors

They include HOMO, LUMO, energy gap (E_g), chemical hardness (η), electronegativity (X), chemical potential (V), electrophilicity (ω), electron affinity (A), ionization potential (I) and global softness (S) which are calculated at B3LYP/6-311G (d, p). The frontier molecular orbital (FMO) energies were calculated for the studied compounds at the same level of theory. The electron donating ability characterized by HOMO energy, while LUMO energy characterizes the electron withdrawing ability. The molecular chemical stability characterizes by Energy gap (E_g) between HOMO and LUMO which is a critical parameter in determining molecular electrical transport properties because it is a measure of electron conductivity. The results in Figure 2, 3 and Table 3 indicate that the smaller the energy gap, the easier the charge transfer, which results in polarization of the molecule. Furthermore, the order of increasing reactivity in the studied compounds is: **1 > 2 > 4 > 3.** Using HOMO and LUMO energies, ionization potential and electron affinity can be expressed as I~ $-E_{HOMO}$, A~ $-E_{LUMO}$ at the B3LYP/6-311G (d,p) as shown in (Table 3). The variation of electronegativity (X) values is supported by electrostatic potential, for any two molecules, where electron will be partially transferred from one of low X to that of high X. The results show that the order of decreasing X is: **1 > 3 > 2 > 4**. The results of small η values for the studied compounds reflect the ability of charge transfer inside the molecule. Therefore, the order is: **3 > 1 > 2 > 4**.

There is a linear relationship between η and E_g as shown in (Table 3). Considering η values, the higher the η values, the harder is the molecule and vice versa.

3.1.4. Natural Charge

The natural population analysis [39] performed on the electronic structures of compounds **1-4** clearly describes the distribution of electrons in various sub-shells of their atomic orbits. The accumulation of charges on the individual atom presented in Table 2. In case of our studied compounds **1-4**, the most negative centers are O1, O2, O3, O4, O5, N1, N2, and N3 -atoms. According to an electrostatic point of view of the molecule, these negative atoms have a tendency to donate an electron. Whereas, the most electropositive atoms such as; Cl have a tendency to accept an electron.

3.2. Nonlinear optical (NLO) Analysis

No experimental or theoretical investigations were found addressing NLO for these classes of molecules; therefore, this triggered our interest to undertake this study. NLO is at the forefront of current research due to its importance in providing key functions of frequency shifting, optical modulation, switching, laser, fiber, optical materials logic and optical memory for the emerging technologies in areas such as telecommunications, signal processing and optical inter connections [40]. To investigate the relationship between the molecular structure and NLO, the polarizibilities and hyperpolarizibilities of the studied compounds 1-4 were calculated using DFT/B3LYP/6-311G (d, p). The total static dipole moment (μ), the mean polarizibility α, the anisotropy of the polarizability Δα, the mean first-order hyperpolarizibility (β) of the studied compounds **1-4** are listed in Table 4. P-nitro aniline (PNA) is a standard prototype used in NLO studies. In this study, PNA is chosen as a reference as there were no experimental values of NLO properties of the studied compounds. The values of α, β in Table 4 illustrate that the order of increasing α with respect to PNA is: compound **4** is higher than (PNA), whereas compounds **2, 1** and **3** are near equal values from the standard (PNA) respectively, The calculated first order hyperpolarizability of p- nitroacetanilide (PNA) is 15.5×10^{-30} esu as reported by T. Gnanasambandan *et al.* [41-43]. The analysis of the β parameter shows that

compounds **1-4** are higher than (PNA). Therefore, the studied compounds **1-4** demonstrate the promising optical properties.

3.3. Molecular Electrostatic Potential (MEP)

The electronic density is related to Molecular electrostatic potential (MEP) and is a very useful descriptor in understanding sites for electrophilic and nucleophilic attack as well as hydrogen bonding interactions [44]. This is correlated with dipole moments, electro negativity, partial charges, and chemical reactivity of the molecules. These maps allow us to visualize the variably charged regions of a molecule. Knowledge of the charge distributions can be used to determine how molecules interact with one another. The calculated 3D MEP and ESP of some of the studied compounds **1-4** are calculated from optimized molecular structure using DFT/B3LYP/6-311G (d, p) are shown in Figure 3 and 4. The results show that, the negative region (red) is mainly over the O and N atomic sites, which is caused by the contribution of lone-pair electron of oxygen atom while the positive (blue) potential sites are around the hydrogen, and carbon atoms. A portion of the molecule that has negative electrostatic potential will be susceptible to electrophilic attack—the more negative the higher the tendency for electrophilic attack. The color scheme for the MEP surface is as follows: red for electron rich, (partially negative charge); blue for electron deficient, (partially positive charge); light blue for (slightly electron deficient region); yellow for (slightly electron rich region); green for neutral (zero potential) respectively. Potential increases in the following order: red < orange < yellow < green < blue [45, 46].

3. 4. Electronic Absorption Spectra of Compound 1

Figure 5 and Table 6 present the experimental and theoretical electronic absorption spectra of **1** in dioxane and ethanol. The experimental spectrum in dioxane as non-polar solvent shows three intense bands at 410 nm, 320 nm, and 297 nm. Increasing solvent polarity on going from dioxane to ethanol gives three bands at 405 nm, 315 nm, and 293 nm. Increasing solvent polarity results in a blue shift with the first band is shifted to 405 nm, the second band is shifted to 315 nm, and the third band is shifted to 293 nm, respectively. The three observed

bands are assigned as (π–π*) transitions, as indicated by the values of molar absorptive (ε = 2400). In order to account for the experimentally observed UV spectra of **1** in dioxane and ethanol, it is essential to consider the theoretically calculated vertical transitions using TD-DFT-CAM-B3LYP/6-311G (d, p) level. The experimental band at 410 nm (in dioxane) is reproduced theoretically by using PCM (dioxane), at 400 (state I) nm, and in gas phase at 399 nm as shown in Table 6. The theoretical calculations of single point energy vertical excitations in ethanol reproduce the wavelength of this band at 402 nm (state I). The second band observed experimentally at 320 nm in dioxane, is reproduced theoretically at 309 nm (state II). The gas phase calculation gives a wavelength at 307 nm. Moreover, in ethanol, this same band appears at 315 nm, where theoretical calculations in ethanol reproduce this band at 310 nm (state II), as depicted in Table 6. The third $(\pi\text{-}\pi^*)^1$ state observed experimentally at 297 nm in dioxane, is reproduced theoretically at 287 nm (state III), which involves the orbital's φ_{85} and $\varphi_{87,}$ in the transition. The gas phase calculation gives a wavelength at 285 nm (state III). In ethanol, this same band appears experimentally at 293 nm, is reproduced theoretically at 289 nm, (state III), as shown in Table 6. The nature of the electronic transition can be inferred from examining the electron density contours of molecular orbitals. The twelve orbital's φ_{76} – φ_{87}, involved in the theoretical transitions of **1**, are shown in Figure 9, show a delocalization of electron density, and Charge Transfer (CT) character.

The NBO analysis of the studied compounds **1-4** provides an efficient method for studying intra-and intermolecular bonding and also provides a convenient basis for investigating charge transfer or conjugative interactions in molecular systems. Table 5 presents the second order perturbation energies of most interacting NBOs of **1-4** and the most important interaction between filled (donor) Lewis type NBOs and empty (acceptor) non-Lewis NBOs. The charge density maps of HOMO and LUMO for **1-4** are presented in Figure 9. The results of NBO analysis of compound **1** tabulated in Table 5 indicate that there is a strong hyper conjugative interactions LP(3) O9 → π*N7-O8, LP(1)N28 → π*C27-O33, LP(2)O35→ π*C34 - O36, LP(2)O36 → π*C34-O35, π*C1-C3 → π*C2-C4, π*C12-C14→ π*C13-C15 and π*C16-

Asian Journal of Nanoscience and Materials

C17→ π*C27-O33, for **1** is 165.94, 55.75, 33.09, 44.48, 191.34, 198.93, and 188.01 kcal/mol, respectively. The C–O π orbital in carboxylic group and benzene ring interacts equally. Furthermore, the lone pair orbital of the oxygen and nitrogen-atoms enjoys hyperconjugation with the C–O, C–N, and C2–C4 π* orbital. It is surprising to notice a decrease in the population of the NBO C1–C3, C12–C14 and C16–C17 reflecting a charge transfer away from the studied compounds **1-4**. In conclusion, **1** enjoys the linear conjugation that is responsible for the observed spectrum. No specific part of the molecule manifests itself in the observed spectrum.

3. 5. Electronic Absorption Spectra of Compound 2

The experimental and theoretical electronic absorption spectra of compound **2** in dioxane and ethanol are shown in Figure 6 and Table 7. In dioxane, the experimental spectrum is composed of two bands, at 385 nm and 260 nm. Increasing solvent polarity from dioxane to ethanol results in a blue shift of the two bands, where the first band is shifted to 380 nm, the second band is shifted to 255 nm respectively. Furthermore, increasing solvent polarity causes a marked increase in the intensity of both bands. The three observed bands are assigned as (π–π*) transitions, based on the values of molar absorptive (ε = 2600). Interpretation of the experimentally observed UV spectra of **2** in dioxane and ethanol requires the theoretical calculations of the vertical transitions using CAM/B3LYP/6-311G (d, p) level. In dioxane, the band appearing in the experimental spectrum at 385 nm is reproduced theoretically using dioxane as a solvent at 372 nm (state I), as shown in Table 7, which involves orbital's φ_{86} to φ_{87}, showing a good agreement between the observed wavelength with the calculated wavelength. Theoretical gas phase calculations of compound **2** give a vertical excitation at 370 nm (state I), which is about 15 nm lower than the experimental wavelength, where the transition in the gas phase also involves the same orbitals. Increasing solvent polarity results in a blue shift of λ_{max} of this band to 380 nm. The theoretical calculations of the vertical excitation in ethanol reproduce the wavelength of this band at 378 nm (state I), indicating that the orbital's φ_{86} to φ_{87} are involved in this transition. It is also clear that the calculated wave length is lower than the

observed wavelength. The second band observed experimentally in dioxane at 260 nm, is reproduced theoretically at 250 nm (state II), indicating that the orbital's φ_{80} to φ_{87} are involved in this transition. Theoretical gas phase calculations give a wavelength at 248 nm (state II). This same band is observed at 255 nm in ethanol, where theoretical calculations in ethanol reproduces this band at 250 nm (state II), which is lower than the observed wavelength, where the orbital's φ_{80} to φ_{87} are involved in this transition. The nature of the electronic transition can be inferred from examining the electron density contours of molecular orbitals. The 13 orbital's φ_{79} – φ_{91} involved in the theoretical transitions of **2**, are demonstrates in Figure 9, show a localization and delocalization of electron density, and charge transfer (CT) character.

The results of NBO analysis of compound **2** tabulated in Table 5 indicate that there is a strong hyper conjugative interactions LP(1)N35→C33-O34, LP(2)O41→ π*C40-O42, LP(2)O42 → π*C40-O41 and π*C1-C3 → π*C5-C6, for **2** is 50.22, 31.49, 46.68, and 264.42 kcal/mol, respectively. NBO analysis of compound **2** Table 5 indicates that it retained the extended conjugation of **1** as revealed by the interaction of C–O and C–N NBOs with those of benzene ring. Furthermore, the interaction of the oxygen and nitrogen lone orbital's with C–O, C–N, and C2–C4 π* orbital is marked. The population of the NBO C1–C3, reflecting a charge transfer away from the studied compounds **1-4**. This is also evident in the case of the population of the oxygen lone orbital LP(1)N35.

3. 6. Electronic Absorption Spectra of Compound 3

The experimental and theoretical electronic absorption spectra of compound **3** in dioxane and ethanol are shown in Figure 7 and Table 8. The experimental spectrum in dioxane is composed of three bands at 350 nm, 293 nm, and 220 nm. The change of solvent polarity from dioxane to ethanol results in a red shift of the three bands, where the first band is shifted to 355 nm, the second band is shifted to 298 nm, and the third band is shifted to 225 nm, respectively. Furthermore, increasing solvent polarity causes a marked increase in the intensity of both bands. The values of molar absorptive (ε = 2400) indicates that the three observed bands have π–π* character.

Asian Journal of Nanoscience and Materials

Theoretical transitions in the gas phase give a vertical excitation at 344 nm (state I), which is about 6 nm lower than the experimental wavelength, where it involves the same orbitals as in dioxane. Theoretical vertical excitation calculations in ethanol give λ_{max} of this band at 343 nm (state I), which shows agreement, implying that the orbitals involved in this transition are φ_{82} to φ_{83}. The experimental second band observed at 293 nm in dioxane, is reproduced theoretically at 288 nm (state II), where the calculations in dioxane indicate that the same orbital's are involved in this transition. Gas phase calculations give λ_{max} at 286 nm (state II). Theoretical calculations in ethanol show that, this band appears at 289 nm (state II), which is lower than the experimental wavelength. The third $(\pi\text{-}\pi^*)^1$ state observed experimentally at 220 nm in dioxane, is reproduced theoretically at 215 nm (state III), which involves the orbital's φ_{80} to $\varphi_{85,}$ in the transition. The gas phase calculation gives a wavelength at 218 nm (state III). In ethanol, this same band appears experimentally at 225 nm, is reproduced theoretically at 217 nm, (state III), as shown in Table 8. The nature of the electronic transition can be inferred from examining the electron density contours of molecular orbital's. The 11 orbital's $\varphi_{76} - \varphi_{86}$, involved in the theoretical transitions of **3**, are shown in Figure 9, show a localization and delocalization of electron density, and CT character.

The results of NBO analysis of compound **3** tabulated in Table 5 indicate that there is a strong hyper conjugative interactions πC1-C3 → π*C5-C6, πC9-C11→ π*C13-C14, π*C1-C3 → π*C5-C6 and π*C13-C14→π*C25-O26, for **3** is 19.36, 23.45, 234, and 168.5 kcal/mol, respectively. NBO analysis of compound **3** Table 5 indicates that it retained the extended conjugation of **1** as revealed by the interaction of C–O and C–N NBOs with those of benzene ring. Furthermore, the interaction of the oxygen and nitrogen lone orbital's with C–O, C–N, and C2–C4 π* orbital is marked. The population of the NBO C13–C14, and C1–C3 reflecting a charge transfer away from the studied compounds **1-4**.

3. 7. Electronic Absorption Spectra of Compound 4

The experimental and theoretical electronic absorption spectra of compound **4** in dioxane and ethanol are shown in Figure 8 and Table 9. The experimental

spectrum in dioxane is composed of three bands at 360 nm, 290 nm, and 255 nm. The change of solvent polarity from dioxane to ethanol results in blue shift to 355 nm, 285 nm and 250 nm respectively. Additionally, increasing solvent polarity causes a marked increase in the intensity of both bands. The values of molar absorptive (ε = 2400) indicates that the three observed bands have π–π* character. The theoretical transition of the first band in dioxane involves orbital's φ_{86} to φ_{87}, showing a good agreement between the observed and the calculated wavelengths. Theoretical transitions in the gas phase give a vertical excitation at 353 nm (state I), where it involves the same orbital's as in dioxane. Theoretical vertical excitation calculations in ethanol give λ_{max} of this band at 350 nm (state I). The experimental second band observed at 290 nm in dioxane, is reproduced theoretically at 282 nm (state II), where the calculations in dioxane indicate that the orbital's φ_{83} and φ_{87} are involved in this transition. Gas phase calculations give λ_{max} at 280 nm (state II). Theoretical calculations in ethanol show that, this band appears at 284 nm (state II). The third $(\pi\text{-}\pi^*)^1$ state observed experimentally at 255 nm in dioxane, is reproduced theoretically at 246 nm (state III), which involves the orbital's φ_{83} and $\varphi_{88,}$ in the transition. The gas phase calculation gives a wavelength at 248 nm (state III). In ethanol, this same band appears experimentally at 250 nm, is reproduced theoretically at 247 nm, (state III), as illustrated in Table 9. The nature of the electronic transition can be inferred from examining the electron density contours of molecular orbital's. The 12 orbital's φ_{80} – φ_{91}, involved in the theoretical transitions of **4**, are shown in Figure 9, show a localization and delocalization of electron density, and the CT character.

The results of NBO analysis of compound **4** tabulated in Table 5 indicate that there is a strong hyper conjugative interactions πC2-C4→π*C1-C3, πC5-C6→π*C1-C3, πC10-C12→π*C9-C11,π*C1-C3→ π*C2-C4, and π*C13-C14 → π*C25-O26, for **4** is 22.16, 21.33, 20.83, 137.13 and 168.5 kcal/mol, respectively. NBO analysis of compound **4** Table 5 indicates that it retained the extended conjugation of **1** as revealed by the interaction of C–O and C–N NBOs with those of benzene ring. Furthermore, the interaction of the oxygen and nitrogen lone orbital's with C–O, C–N, and C2–C4 π* orbital is marked. The population of

Asian Journal of Nanoscience and Materials

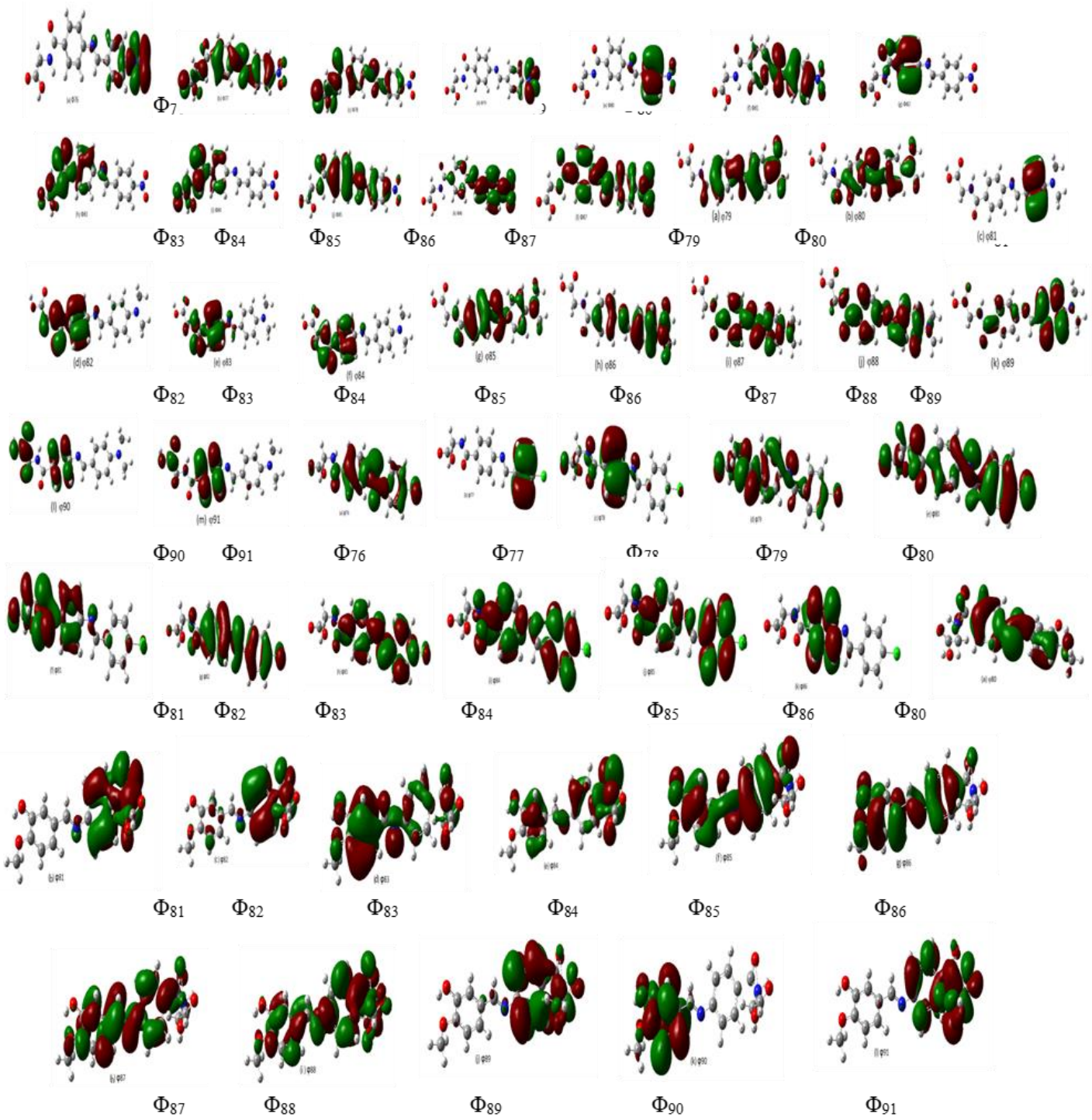

Fig. 9. Electron density contours of the studied compounds **1-4**.

the NBO C13–C14, and C1–C3 reflecting a charge transfer away from the studied compounds **1-4**.

3.10. Biological Activity

The biological activity of the studied compounds **1-4** was tested against

Asian Journal of Nanoscience and Materials

Grame positive bacteria, Grame negative bacteria with Ampicillin and Fungi with Colitrimazole as standard reference for each respectively as shown in Table 10 and Fig. 10. Concerning Grame positive bacteria, two types of bacteria were used in the testing procedure, which are S.aureus and B.subtillis. The compound **3** was less to moderate biologically active compared to other compounds, while the compound **4** showed high biological activity. Compounds **1** and **2** were moderately active compared to **4**. The order of Grame positive bacteria; **4 > 2 > 1 > 3.** Concerning Grame negative bacteria, two types of bacteria were also used in the testing procedure, which are Pseudomonas aeuroginosa and E.coli. The compound **3** depicted less to moderate biological activity compared to standard reference. On the other hand, the compound **2** showed high biological response, compounds **1** and **4** were moderately active. The order of Grame negative bacteria; **2 > 4 > 1 > 3.** Moving to Fungi, C.albicans and A.flavus were the two types used in the testing procedure. The compound showed less to moderate **3** biological activity. Compound **1** showed moderate in the biological activity, compounds **4** and **2** showed high biological activity. The order of Fungi; **4 > 2 > 1 > 3.**

The studied compounds can be arranged according to their biological activity against Grame positive bacteria, Grame negative bacteria and Fungi compared to standard reference as follows: Compounds **2** and **4** comes first with the highest biological activity, than compound **1** compound **3** is the last one with the least biological activity.

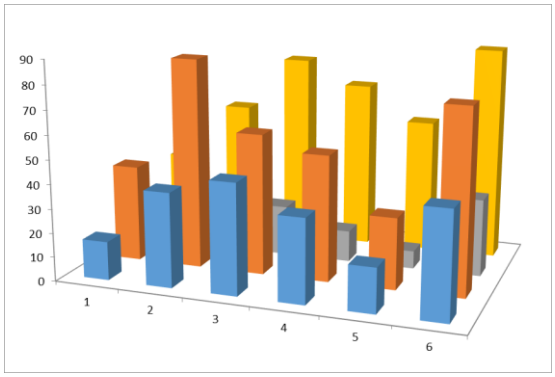

Fig. 10. Antimicrobial activity for the studied compounds **1-4** against gram-positive bacteria (G^+), gram-negative bacteria (G^-), and Fungi (F).

3.11. Correlation Between Biological and Ground State Properties

The biological activity of the studied compounds **1-4** can be correlated with the ground state energetic and global properties. From the computed data in Table 3, one can reveal the following: The biological activity of the studied compound obtained experimentally follow the order **4 > 2 > 1 > 3**, Against G+, and fungi while G- follow the order **2 > 4 > 1**

> 3 . The theoretical polarity, μ, of the studied compound computed at B3LYP/6-311G (d, p) follow the same order obtained experimentally indicating that μ is one factor contributing to the polarity of the studied compounds (c.f. Table 3). The theoretically computed chemical hardness (η), electronegativity (χ), chemical potential (V), the theoretical chemical reactivity, Eg, the global softness (S), and global electrophilicity index, (ω), and natural charge from NBO of the studied compounds; follow the reverse order of the experimental biological activity. In case of the mean first-order hyperpolarizability (β), the order are **1 > 2 > 4 > 3** which violate the order of the experimental biological activity.

Conclusion

Electronic structure of componds **1-4,** were investigated theoretically at B3LYP/6-311G (d, p). All the studied compounds were found to be non-planar. The ground state properties of **1-4** revealed that the compound **1** had the lowest E_{HOMO}, E_{LUMO}, and E_{gap} indicating highest reactivity. From the computed dipole moment, compound **4** is found to have the highest polarity. Also, the Mullikan and natural charge distribution of the compounds **1–4** were studied which indicated the electronic charge distribution. The calculated dipole moment and first order hyperpolarizability results indicate that the molecule has a reasonable good non-linear optical behavior. MEP confirmed the different negative and positive potential sites of the molecule in accordance with the total electron density surface. Electronic absorption spectra were investigated experimentally in dioxane and ethanol; and theoretically in gas phase, dioxane and ethanol using CAM-B3LYP/6-311G (d, p). The band maxima (λ_{max}) and intensities of the spectra are found to have solvent dependence. The bands of compounds **1, 2,** and **4** showed blue shift, while compounds **3** show red shift. The NBO analysis of the compounds **1–4** indicated the intermolecular charge transfer between the bonding and antibonding orbital's. The biological activity of the studied compounds show that compound **4** was the most active one ,whereas, the molecule **3** is the least active and the order of reactivity is **4 > 2 > 1 > 3.**

Conflicts of Interest

The manuscript does not include a conflict of interest, and there is no funded entity for this research study.

References

1. Cimerman, Z., Miljanić, S., & Galić, N. (**2000**). *Croat Chem Acta*. **73**:81-95.
2. Ghorbani-Choghamarani, A., Tahmasbi, B., Arghand, F., & Faryadi, S. (**2015**). *RSC Adv*, **112**: 92174-92183.
3. Nikoorazm, M., Ghorbani- Choghamarani, A., & Noori, N. (**2015**). *Appl Organomet Chem*. **5**: 328-333.
4. Kabak, M., Elmali, A., & Elerman, Y. (1999). *J Mol Struct*, 477(1), 151-158.
5. Patel, P. R., Thaker, B. T., & Zele, S. (**1999**). Preparation and characterisation of some lanthanide complexes involving a heterocyclic β–diketone.
6. Nikoorazm, M., Ghorbani-Choghamarani, A., Panahi, A., Tahmasbi, B., & Noori, N. (**2018**). *J Iran Chem Soc* .1:181-189.
7. Nikoorazm, M., Ghorbani, F., Ghorbani-Choghamarani, A., & Erfani, Z. (**2018**). *Phosphorus Sulfur*, 1-10.
8. M. Nikoorazm, Ghorbani-Choghamarani, A., & Khanmoradi, M. (**2016**). RSC Adv, 61: 56549.
9. Raman, N., Raja, Y. P., & Kulandaisamy, A. (**2001**). J . Chemical Sciences, 113(3), 183-189.
10. Khanmoradi, M., Nikoorazm, M., & Ghorbani- Choghamarani, A. (**2017**). *Appl Organomet Chem*, 9 : e3693.
11. Ghorbani- Choghamarani, A., Darvishnejad, Z., & Norouzi, M. (**2015**) .*Appl Organomet Chem*, 10: 707-711.
12. ASHRAF¹, M. A., Wajid, A., Mahmood, K., MAAH¹, M. J., & Yusoff, I. (**2011**. Oriental Journal of Chemistry, 2: 363-372.
13. Ghorbani- Choghamarani, A., Darvishnejad, Z., & Norouzi, M. (2015). *Appl Organomet Chem*, 3: 170-175.
14. Ghorbani-Choghamarani, A., Darvishnejad, Z., & Tahmasbi, B. (**2015**). Inorg Chimi Acta, 435 : 223-231.
15. Campos, A., Anacona, J. R., & Campos-Vallette, M. M. (**1999**).

Main Group Metal Chemistry, 22: 283-288.

16. Sari, N., Arslan, S., Logoglu, E., & Sakiyan, I. (**2003**). GUJ Sci, 1:283-288.
17. ASHRAF¹, M. A., Wajid, A., Mahmood, K., MAAH¹, M. J., & Yusoff, I. (**2011**).Oriental Journal of Chemistry, 27: 363-372.
18. Cozzi, P. G. (**2004**). *Chem. Soc. Rev*, 33: 410-421.
19. CHANDRA, S. (**2004**). Journal of the Indian Chemical Society, 81: 203-206.
20. Pandeya, S. N., Yogeeswari, P., Sriram, D., De Clercq, E., Pannecouque, C., & Witvrouw, M. (**1999**). Chemotherapy, 45:192-196.
21. Nikoorazm, M., Ghorbani-Choghamarani, A., & Noori, N. (**2015**). Journal of Porous Materials, 22: 877-885.
22. Becke, A. D. (**1993**). The Journal of chemical physics, 98: 5648-5652.
23. Lee, C., Yang, W., & Parr, R. G. (**1988**). Physical review B, 37: 785.
24. Frisch, M. J., Trucks, G. W., Schlegel, H. B., Scuseria, G. E., Robb, M. A., Cheeseman, J. R., ... & Millam, J. M. Komaromi, RL Martin, DJ Fox, T. Keith, MA Al-Laham, CY Peng, A. Nanayakkara, M. Challacombe, PMW Gill, B. Johnson, W. Chen, MW Wong, C. Gonzalez, JA Pople, Gaussian, 3.
25. Frisch, M. J. E. A., Trucks, G. W., Schlegel, H. B., Scuseria, G. E., Robb, M. A., Cheeseman, J. R., ... & Nakatsuji, H. (2009). Gaussian 09, revision a. 02, gaussian. Inc., Wallingford, CT, 200.
26. http://www.chemcraftprog.com.
27.
28. Avcı, D. (**2011**). Molecular and Biomolecular Spectroscopy, 82: 37-43.
29. Avcı, D., Başoğlu, A., & Atalay, Y. (**2010**). Structural Chemistry, 21: 213-219.
30. Avci, D., HÃ¼seyin, C. Ã., & Atalay, Y. (2008). Ab initio Hartree-Fock calculations on linear and second-order nonlinear optical properties of new acridine-benzothiazolylamine chromophores. Journal of molecular modeling, 14(2).

31. Pearson, R. G. (**1986**). Proceedings of the National Academy of Sciences, 83: 8440-8441.
32. Günay, N., Pir, H., Avcı, D., & Atalay, Y. (**2012**). NLO and NBO analysis of sarcosine-maleic acid by using HF and B3LYP calculations. Journal of Chemistry, 2013.
33. J.G. Matecki, (**2010**) Trans. Met. Chem. 35: 801.
34. Yanai, T., Tew, D. P., & Handy, N. C. (**2004**). Chemical Physics Letters, 393: 51-57.
35. Chocholoušová, J., Špirko, V., & Hobza, P. (**2004**). *Physical Chemistry Chemical Physics*, 6: 37-41.
36. Szafran, M., Komasa, A., & Bartoszak-Adamska, E. (**2007**). Journal of molecular structure, 827: 101-107.
37. Macoonald, J. N., Mackay, S. A., Tyler, J. K., Cox, A. P., & Ewart, I. C. (**1981**). J. Chem. Soc. Farady Trans. II, 77: 79-89.
38. D.Y. Sajan, R. Erdogdu, O. Reshmy, K. Dereli, K. Thomas, I. Hubert Joe Spectrochimica Acta Part A 82 (2011) 118-128.
39. Reed, A. E., Weinstock, R. B., & Weinhold, F. (**1985**). Natural population analysis. The Journal of Chemical Physics, 83: 735-746.
40. Bradshaw, D. S., & Andrews, D. L. (**2009**). Quantum channels in nonlinear optical processes. Journal of Nonlinear Optical Physics & Materials, 18: 285-299.
41. Cheng, L. T., Tam, W., Stevenson, S. H., Meredith, G. R., Rikken, G., & Marder, S. R. (**1991**). The Journal of Physical Chemistry, 95: 10631-10643.
42. Kaatz, P., Donley, E. A., & Shelton, D. P. (1998). A comparison of molecular hyperpolarizabilities from gas and liquid phase measurements. The Journal of chemical physics, 108(3), 849-856.
43. Rajesh, P., Gunasekaran, S., Gnanasambandan, T., & Seshadri, S. (**2015**). Spectrochimica Acta Part A: Molecular and Biomolecular Spectroscopy, 137: 1184-1193.
44. Scrocco, E., & Tomasi, J. (**1978**). (Vol. 11, pp. 115-193). Academic Press.

Asian Journal of Nanoscience and Materials

45. Politzer, P., & Murray, J. S. (**2002**). Theoretical Chemistry Accounts, 108: 134-142.
46. Sajan, D., Joseph, L., Vijayan, N., & Karabacak, M. (**2011**). *Molecular and Biomolecular Spectroscopy*, 81: 85-98

How to cite this manuscript: Shimaa Abdel Halim*, Esam A. Gomaa, Shymaa E. Rashed. TD-DFT Calculations, Electronic Structure, NBO, NLO Analysis, Biological Activity, and Electronic Absorption Spectra of Some Novel Schiff base Derivatives. Asian Journal of Nanoscience and Materials, 2019, **2**(2), 159-185. DOI: 10.26655/ajnanomat.2019.3.4